

Supporting Information

Degradation of Hole Transport Materials via Exciton-Driven Cyclization

Bruce M. Bell,[†] Michael B. Clark, Jr.,[‡] David D. Devore,^{*,†} Timothy S. De Vries,^{*,†} Robert D. Froese,[†] Kaitlyn C. Gray,[§] David H. K. Jackson,[¶] T. F. Kuech,[¶] Hong-Yeop Na,[#] Kenneth L. Kearns,[†] Kyung-Joo Lee,[#] Sukrit Mukhopadhyay,[†] Aaron A. Rachford,^{||} Liam P. Spencer,^{††} W. H. Hunter Woodward[†]

[†]Core Research and Development, The Dow Chemical Company, Midland, MI 48674, United States;

[‡]Core Research and Development, The Dow Chemical Company, Collegeville, PA 19426, United States;

[§]Dow AgroSciences, Indianapolis, IN 46268, United States; [¶]Department of Chemical and Biological Engineering, University of Wisconsin-Madison, Madison, WI 53706, United States; [#]Electronic Materials Research and Development, The Dow Chemical Company, Hwasung 445-170, South Korea; ^{||}Electronic Materials Research and Development, The Dow Chemical Company, Marlborough, MA 01752, United States; ^{††}Core Research and Development, The Dow Chemical Company, Freeport, TX 77541, United States.

Corresponding Authors

*E-mail: tsdevries@dow.com, dddevore@dow.com

COMPUTATIONAL METHODOLOGY FOR CALCULATING BOND DISSOCIATION ENERGY (BDE)

Density functional theory (DFT) is used to compute the BDE of isolated HTL molecules in neutral state. Within the realm of DFT, the standard hybrid functional (B₃LYP)¹ with 6-31g* basis set is used for all the calculations with the Gaussian09 program.²

The schematic representation of calculating BDE in neutral state is illustrated in Figure S1; the BDE of a concerned bond is computed as the energy difference between the radical fragments ($E_{\text{Frag-A}} + E_{\text{Frag-B}}$) and the whole molecule (E_{Molecule}). The radicals are computed in the doublet state (one unpaired electron, unrestricted wavefunction) while the whole molecule is computed a closed shell singlet. This methodology for calculating BDE is only applicable if two separate fragments are formed after the homolytic cleavage of the concerned bond. Geometries of all fragments and whole molecules were confirmed to be minima by additional vibrational frequency calculations.

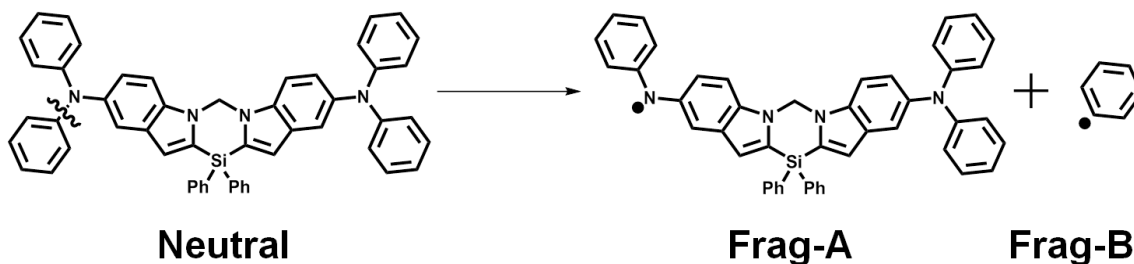


Figure S1. Schematics depicting the methodology for computing the BDE in neutral state of a molecule (the C-N bond is chosen for illustration). The breaking bond (C-N) is indicated by a curly line, the radicals are indicated by “.”.

If the homolytic bond breaking does not lead to two separate fragments such as in a ring system, then bond cleavage will lead to the formation of a labile moiety (with additional degrees of torsional freedom). In such cases, the labile moieties are manually rotated such that the radical pairs are spatially separated from one another. This serves as the initial geometry for the fragmented molecule in neutral state. The energy of the fragmented molecule is computed in the triplet state. The BDE of the concerned bond is obtained by computing the difference in energy between the fragmented and the parent molecule. Such a method of computing BDE is coarse and thus expected to give qualitative estimate of the bond dissociation energies.

It should be pointed out that there is an obvious difference between the bond-breaking processes in Figure S1 and Figure S2. When bond-breaking liberates two molecules (Figure S1), it is likely an irreversible process and the fragments are not likely to come back together. The formed radicals (neutral case) are likely to react in some way, possibly to abstract hydrogen from nearby molecules. When cyclic bond-breaking is done (Figure S2), the reaction is assumed to be reversible and the ring-opened product may be able to react with a nearby molecule but if no such reaction occurs quickly, the bond may reform.

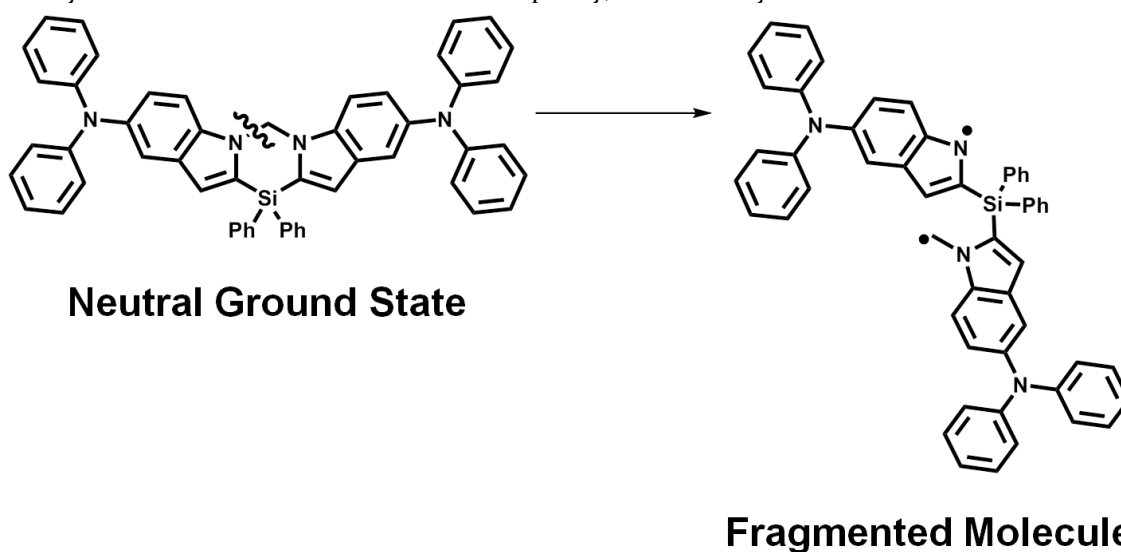


Figure S2. Schematics depicting the methodology for computing the BDE in the neutral state of a molecule (the C-N bond is chosen for illustration), where bond dissociation does not lead to two separate fragments. The concerned bond (C-N) is indicated by a curly line, the radicals are indicated by “.”.

Promising HTL candidates including **1** were evaluated for bond dissociation energy before initiating synthetic efforts by the method described above. Compound **1** was attractive because the N-aryl bonds seemed relatively stable compared to typical HTL molecules NPD and TPD (Figure S3 and Table Si). Bond 3 appears to be relatively weak, but as described above this should not be compared to true fragmentations being part of a ring; two bonds may need to be broken simultaneously for complete fragmentation.

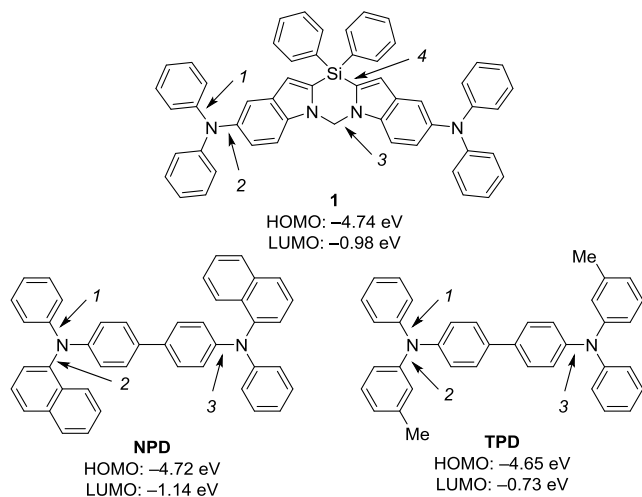


Figure S3. Positions of calculated Bond Dissociation Energies shown in Table 1.

Table Si. Calculated Bond Dissociation Energies (kcal/mol) for **1**, NPD, and TPD.

Bond number	1	NPD	TPD
1	75.2	71.6	75.2
2	76.2	73.6	75.0
3	61.3	73.0	76.9
4	97.9	-	-

COMPUTATIONAL METHODOLOGY FOR CALCULATING TRANSITION STATE ENERGIES

The structures of all the species in ground, triplet (T_1) and transition states (TS) are optimized using Density Functional Theory (DFT) at B3LYP/6-31g*. The geometries of the triplet state were optimized using unrestricted method (using the same functional). The vibrational analysis on the ground state geometries was performed and the lack of imaginary frequencies was used to ascertain the minima in the potential energy surface (PES). On the other hand, the same analysis on the transition state geometries indicated one imaginary frequency. In the latter case, the GaussView program was used to visualize the vibrational mode with imaginary frequency in order to ensure that the atoms move along the desired reaction coordinate. The reactants and the products of cyclization reaction are shown in Figure S4, where the energy of the triplet state, the transition state for cyclization reaction and the dihydro-carbazole intermediate was indicated as E_{T_1} , E_{TS} , $E_{T_1(\text{DHCZ})}$. If the barrier for the forward reaction ($E_{TS} - E_{T_1}$) is high and the cyclization reaction is endothermic ($E_{T_1(\text{DHCZ})} - E_{T_1} = +ve$), the chance for cyclization is minimal. All calculations were performed using G09 suit of programs.²

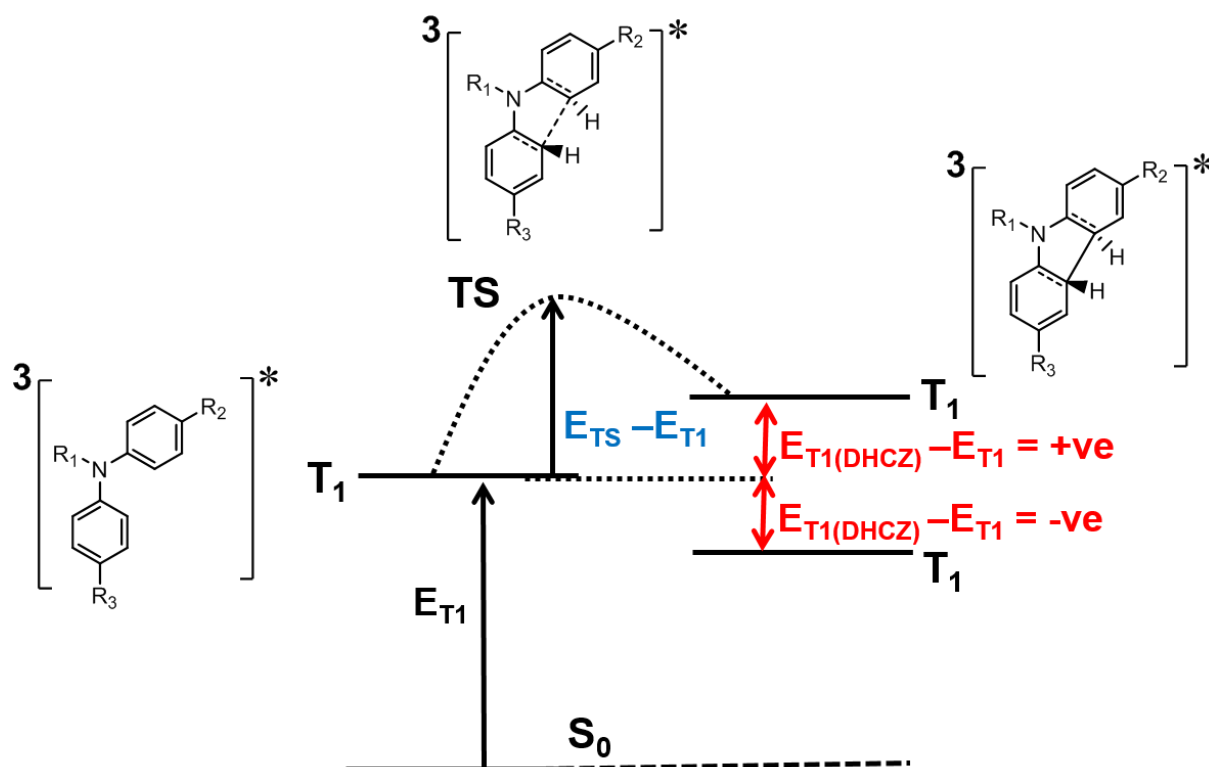
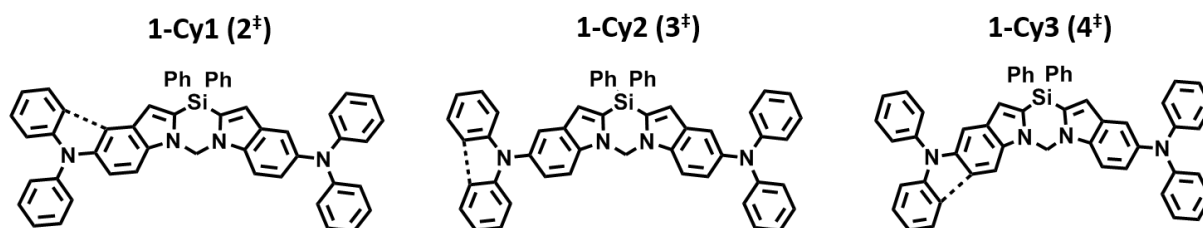
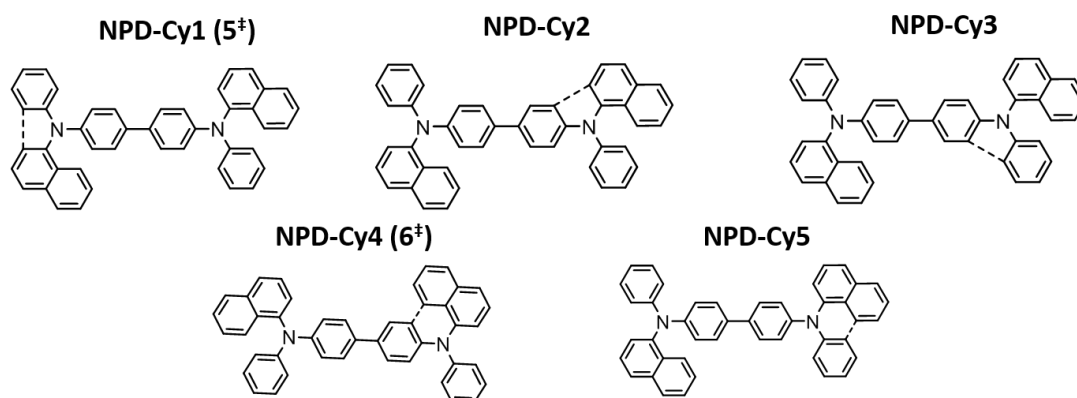


Figure S4. Schematics depicting the methodology for computing the barrier for cyclization ($E_{TS} - E_{T_1}$) and the energetics of the cyclized dihydro-carbazole with respect to the triplet excited state (T_1) of the molecule. R_1 , R_2 and R_3 depend on the chosen HTL.



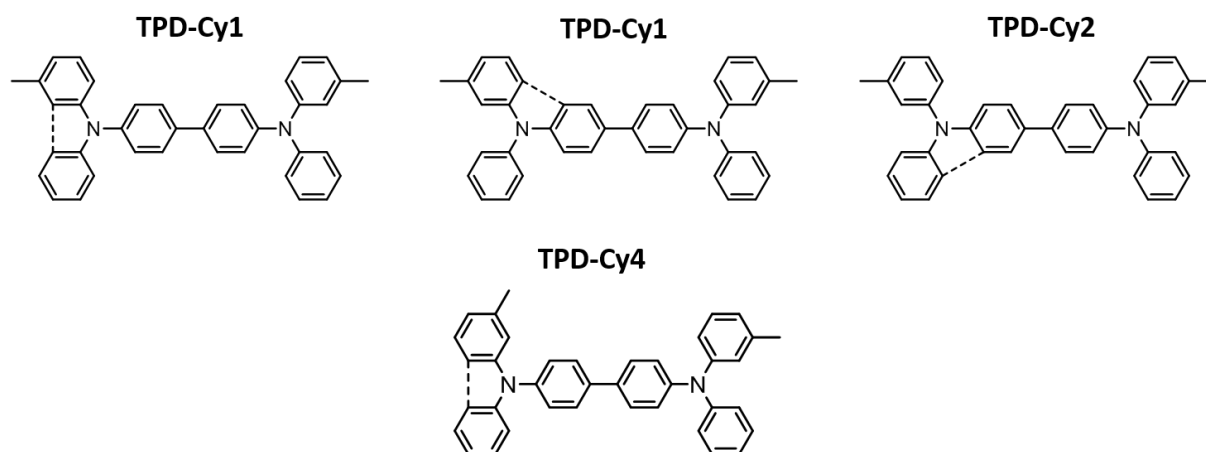
Property	Energy (kcal/mol)		
	1-Cy1 (2 [‡])	1-Cy2 (3 [‡])	1-Cy3 (4 [‡])
$E_{TS} - E_{T1}$	8.0	14.6	14.1
$E_{T1(DHCZ)} - E_{T1}$	-5.8	0.5	-2.6

Figure S5. Molecular structures of cyclized intermediates of HTL1 (Top panel); newly formed bond is shown in dotted line; computed electronic properties to predict rates of cyclization (Bottom panel).



Property	Energy (kcal/mol)				
	NPD-Cy1 (5 [‡])	NPD-Cy2	NPD-Cy3	NPD-Cy4 (6 [‡])	NPD-Cy5
$E_{TS} - E_{T1}$	17.6	17.8	23.5	20.3	20.6
$E_{T1(DHCZ)} - E_{T1}$	7.4	8.1	9.7	0.5	0.2

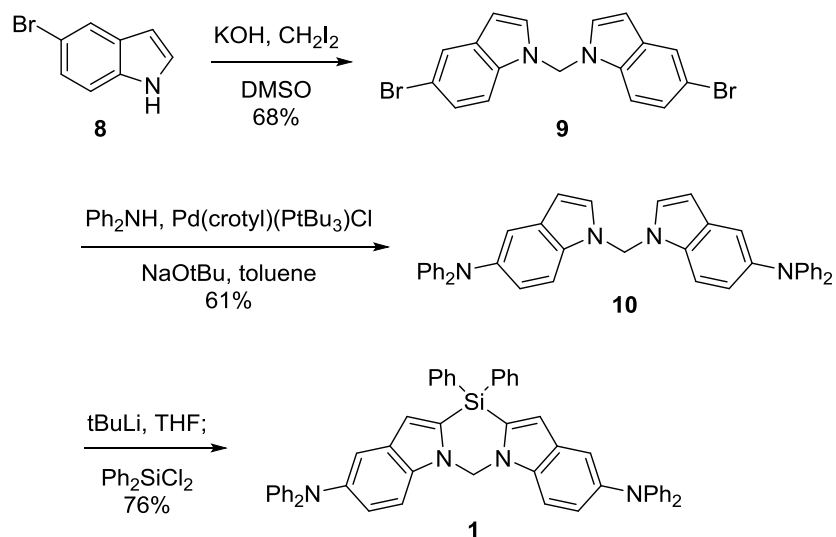
Figure S6. Molecular structures of cyclized intermediates of NPD (Top panel); newly formed bond is shown in dotted line; computed electronic properties to predict rates of cyclization (Bottom panel).



Property	Energy (kcal/mol)			
	TPD-Cy1 (7 [‡])	TPD-Cy2	TPD-Cy3	TPD-Cy4
$E_{TS} - E_{T1}$	20.1	20.3	20.4	20.7
$E_{T1(DHCZ)} - E_{T1}$	6.1	7.0	7.2	6.3

Figure S7. Molecular structures of cyclized intermediates of TPD (Top panel); newly formed bond is shown in dotted line; computed electronic properties to predict rates of cyclization (Bottom panel).

SYNTHETIC ROUTE TO COMPOUND **1**



Scheme S1. Synthetic route to **1**.

NMR SPECTRA OF **9**

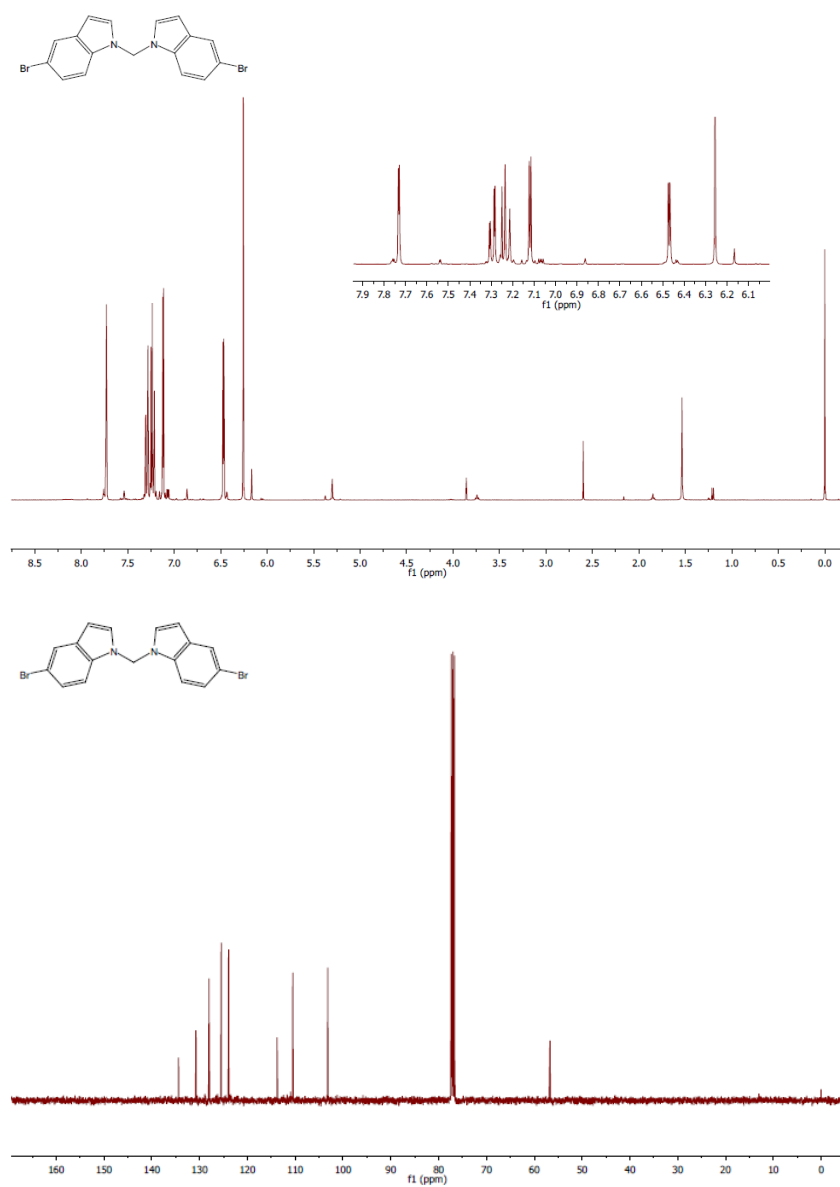


Figure S8. ¹H (top, with inset showing expanded aromatic region) and ¹³C (bottom) NMR spectra of intermediate **9**.

NMR SPECTRA OF **10**

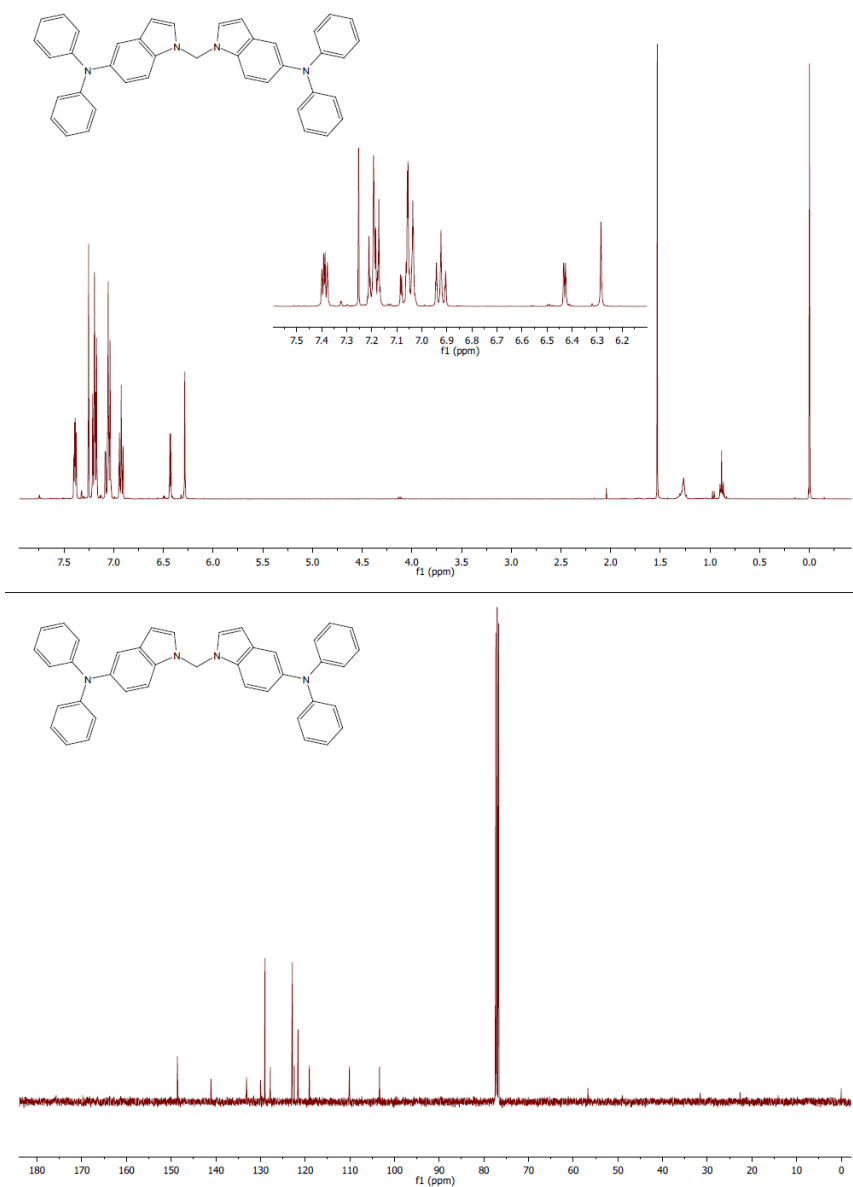


Figure S9. ^1H (top, with inset showing expanded aromatic region) and ^{13}C (bottom) NMR spectra of intermediate **10**.

NMR SPECTRA OF **1**

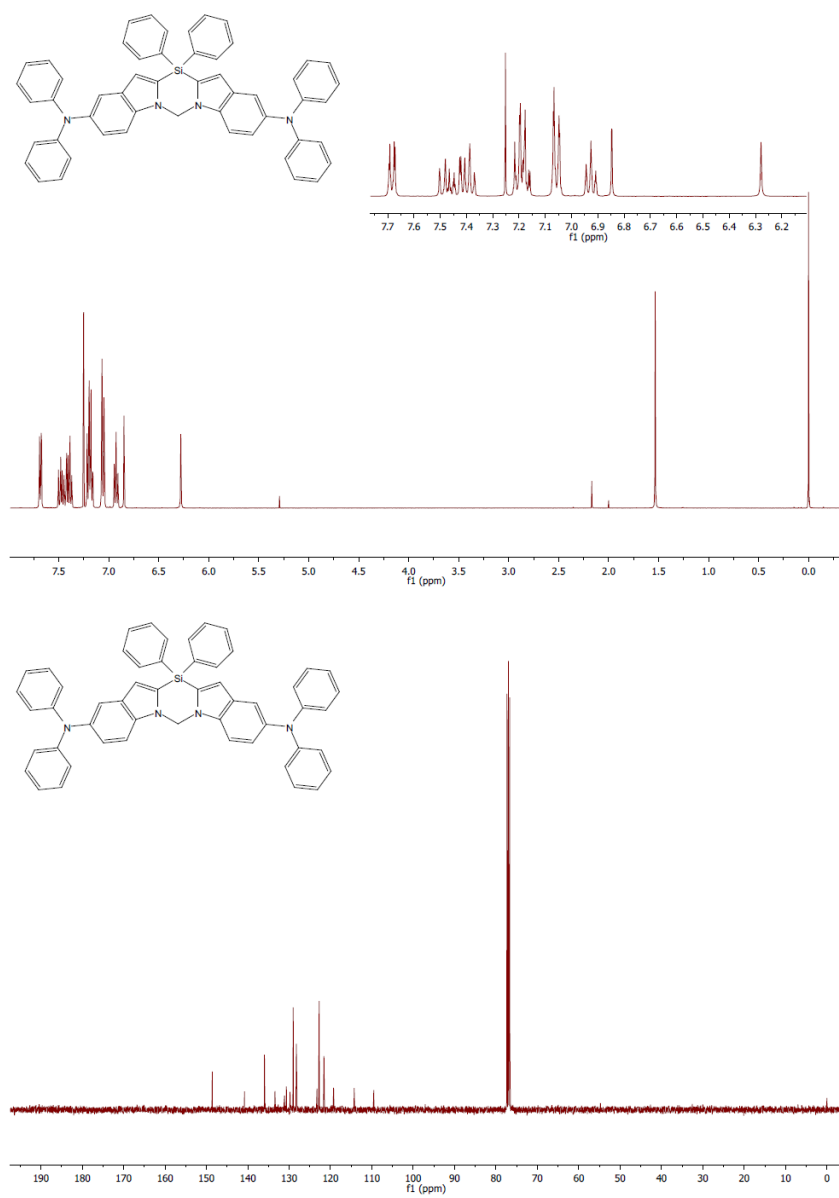


Figure S10. ^1H (top, with inset showing expanded aromatic region) and ^{13}C (bottom) NMR spectra of compound **1**.

IR SPECTRUM OF **1**

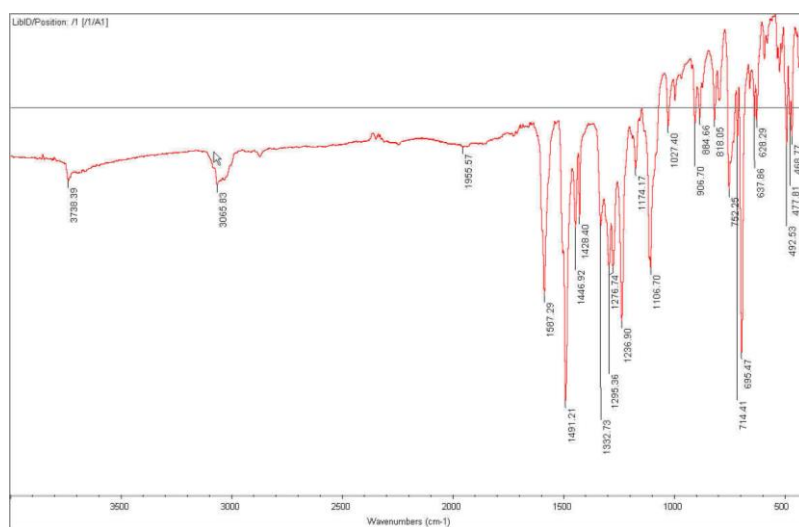


Figure S11. Infrared spectrum (absorbance mode) of compound **1**.

DIFFERENTIAL SCANNING CALORIMETRY DATA FOR **1**

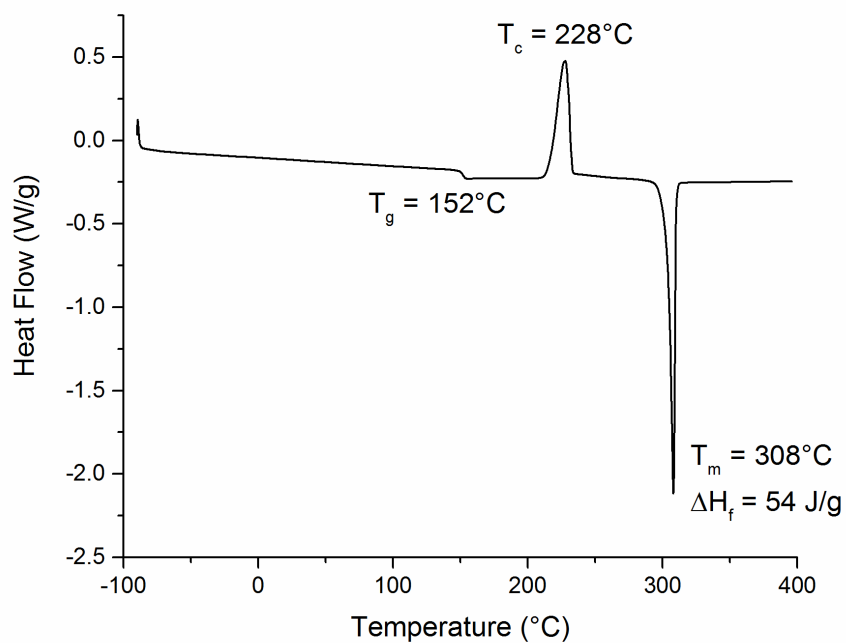


Figure S12. Heat flow versus temperature for compound **1** as measured by differential scanning calorimetry, showing an initial heating cycle.

MATERIALS USED IN OLED DEVICES

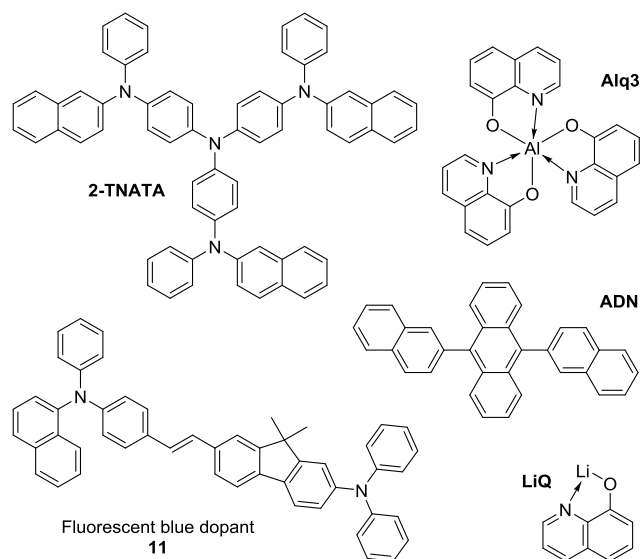


Figure S13. Materials used in fabricated OLED devices.

EL SPECTRA OF DEVICES

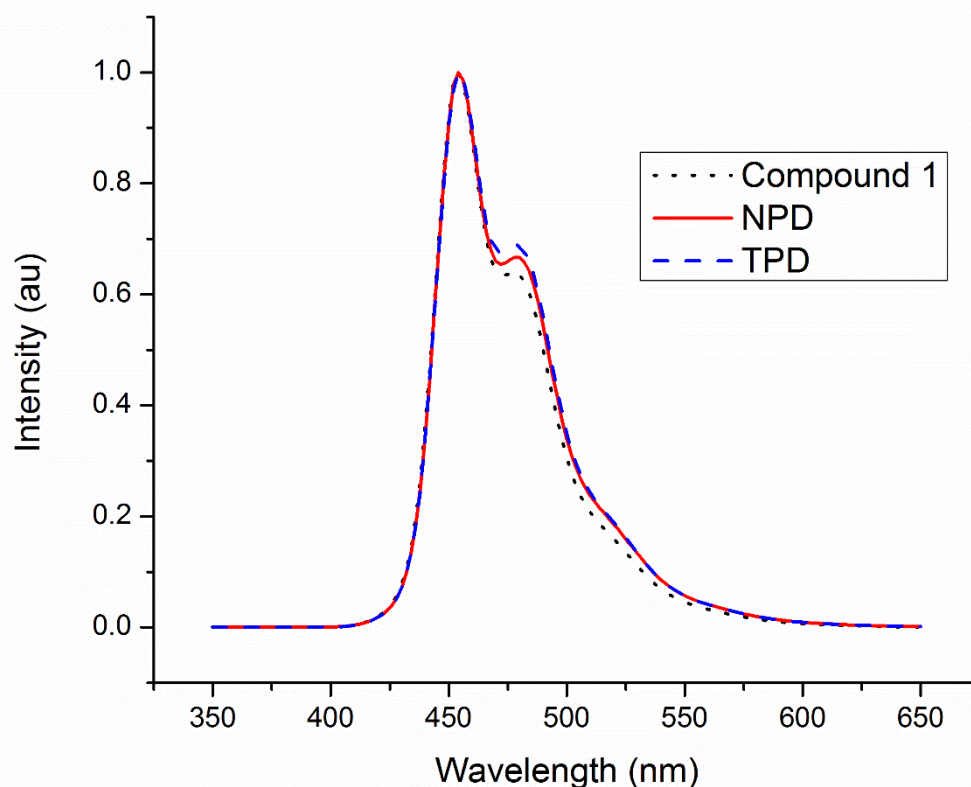


Figure S14. Electroluminescence spectra of devices of the configuration:

ITO / 2-TNATA(60 nm) / HTL(20 nm) / EML(35 nm, 2% dopant in ADN) / Alq₃(20 nm) / LiQ(2 nm) / Al(80 nm)

where HTL is either HTL₁ (black dotted line), NPD (red solid line), or TPD (blue dashed line).

VOLTAGE MEASUREMENT DURING ACCELERATED AGING OF OLED DEVICES

The devices using **1**, NPD, and TPD were aged with acceleration at for 10 hours, driving at constant current determined for each device to provide initial luminance of 3620 cd/m². The change in luminance over time is shown in figure 2c, where the device using **1** as HTL produced only 12% of the initial luminance after 10 hours, compared to NPD or TPD which retained about 89% or 87% luminance, respectively. The voltage required to deliver constant current changed over time as shown in Figure S15.

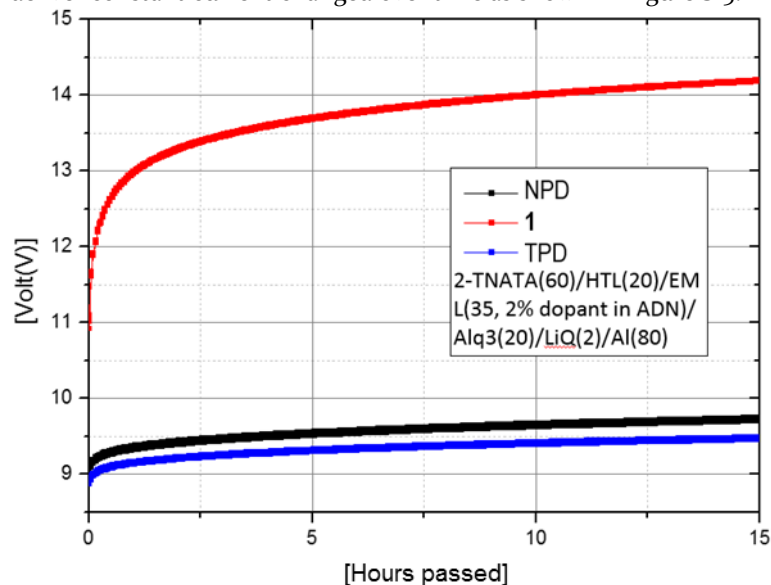


Figure s15. Voltage over time during accelerated aging of OLED devices.

REPRESENTATIVE SIMS DEPTH PROFILE

A typical depth profile, obtained by monitoring the molecular ion (M⁺) intensity from the ETL (electron transport layer), EML, HTL, and HIL (hole injection layer) molecules is plotted in Figure S16 for a device made using TPD as the HTL. The x-axis has been converted from number of sputter cycles to depth, showing good agreement with the intended thickness of each layer.

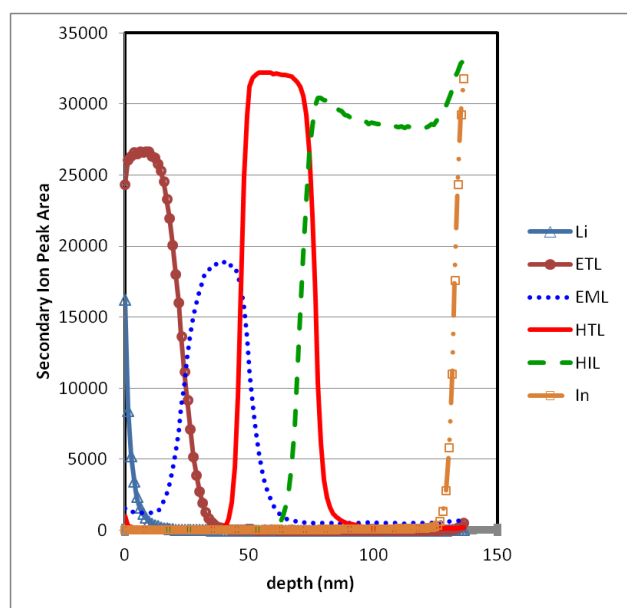
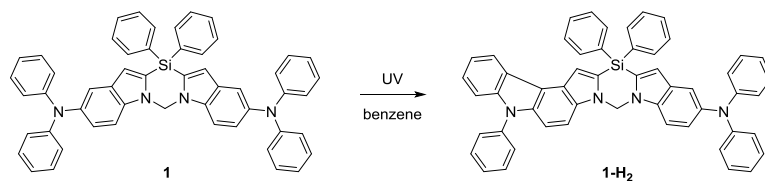


Figure s16. Depth profile of OLED Device using TPD as the HTL.

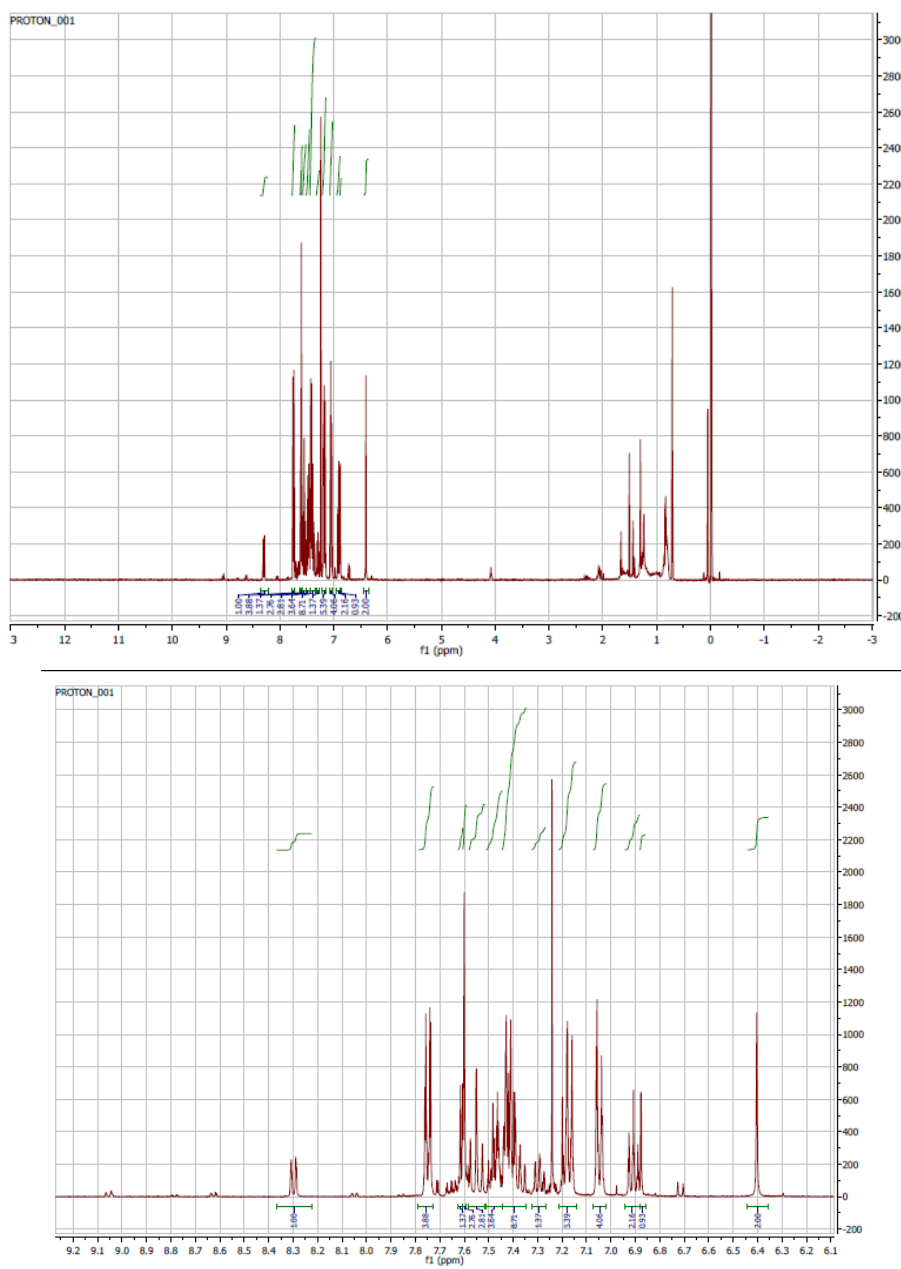
ISOLATION OF CYCLIZATION PRODUCT **1-H₂**



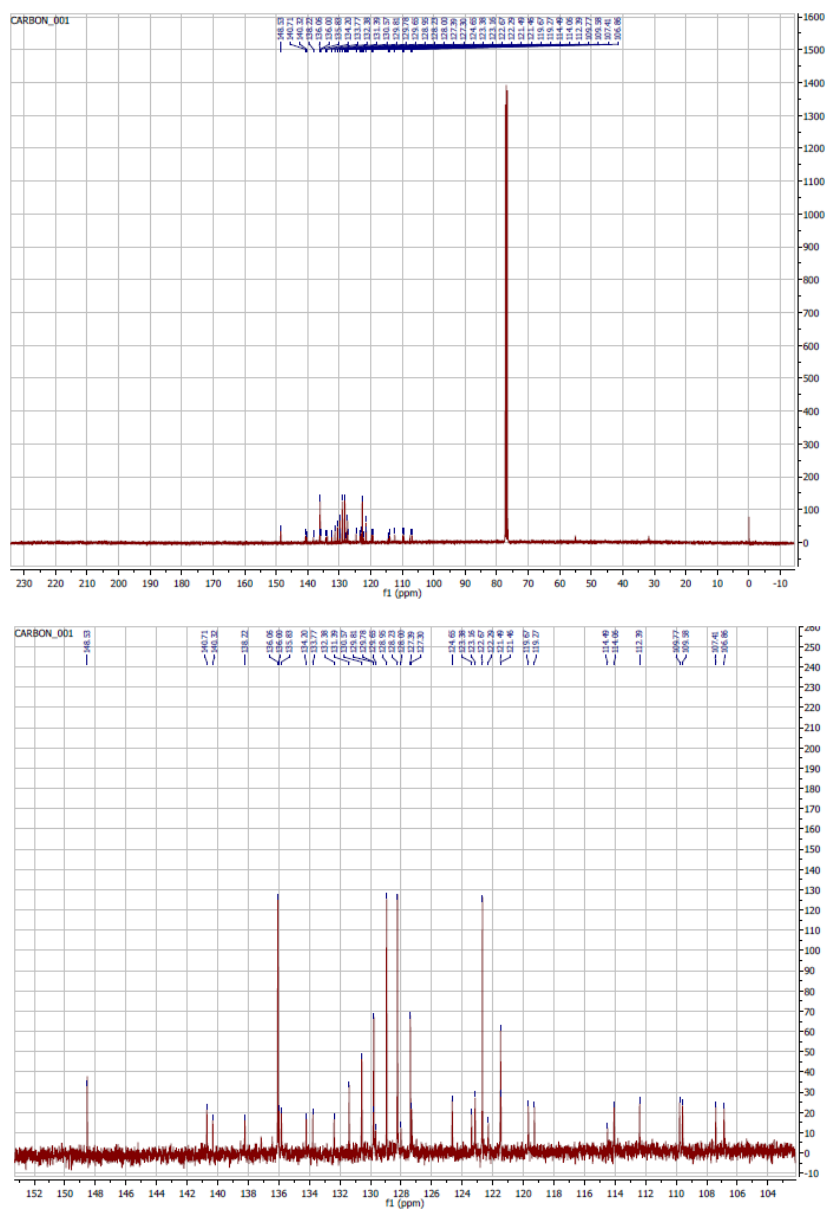
Scheme S2. Putative photocyclization of **1**.

To confirm the identity of the cyclized product, compound **1** was subjected to preparative photolysis. A solution was prepared at slightly higher than usual concentration in benzene (36 mg dissolved into 18 mL benzene) and divided up into 12 NMR tubes, 1.5 mL of solution into each. These were placed around the warmed 450 watt medium pressure mercury lamp for 30 seconds. The samples were combined, concentrated down, and purified by flash chromatography, first reverse phase but combining all fractions containing desired product and resubjecting to normal phase flash chromatography. Solvent residues remained, so the product was put through a plug of silica gel, loading with about 5% chloroform in hexanes (high purity from Fisher Scientific, <2 ppm evaporation residue) and eluting with hexanes, then 1:3 chloroform/hexanes, and finally chloroform – the desired product eluted in chloroform. This was evaporated down to about 2 mg **1-H₂**, with some remaining impurities.

^1H NMR (400 MHz, CDCl_3):



^{13}C NMR (101 MHz, CDCl_3):



IR (thin film): 2927, 1721, 1660, 1596, 1494, 1453, 1429, 1288, 1239, 1108, 699 cm^{-1}

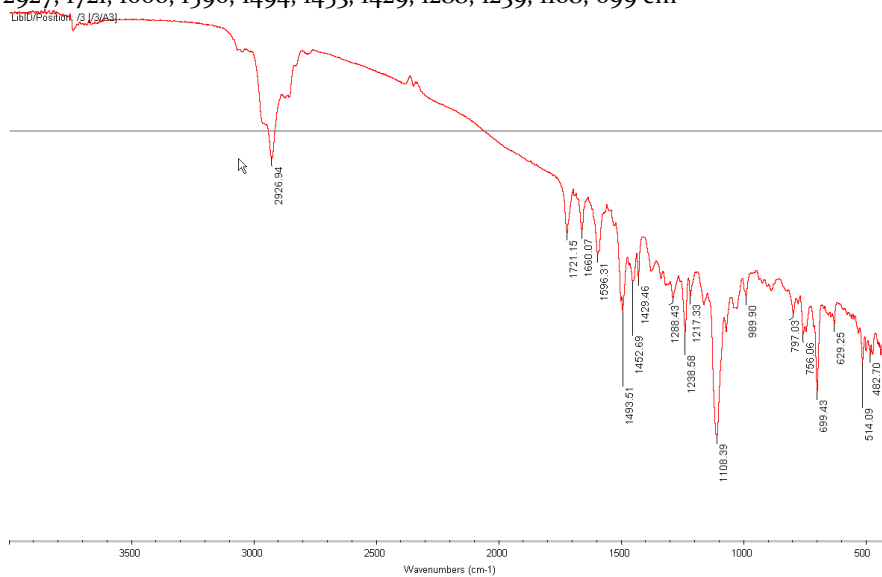


Figure S19. Infrared spectrum (absorbance mode) of **1-H₂**.

HRMS (ESI) m/z : $[M]^+$ calcd for $\text{C}_{53}\text{H}_{38}\text{N}_4\text{Si}$, 758.2866; found, 758.2853.

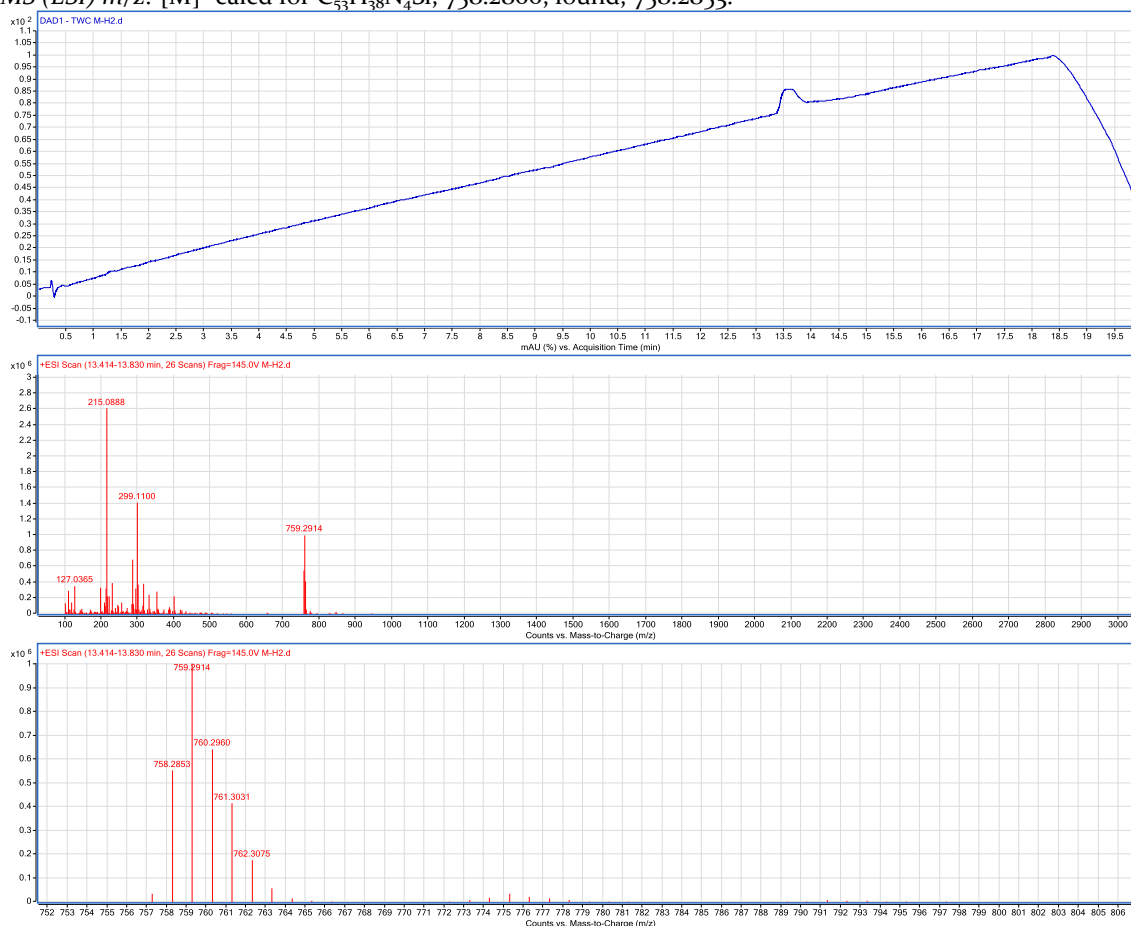


Figure S20. LC/HRMS chromatogram (top) of **1-H₂**, mass spectrum (middle) with expansion to show peak and isotope pattern for $M+H^+$ (bottom).

LC/MS ANALYSES OF PHOTOLYSES OF OTHER MATERIALS

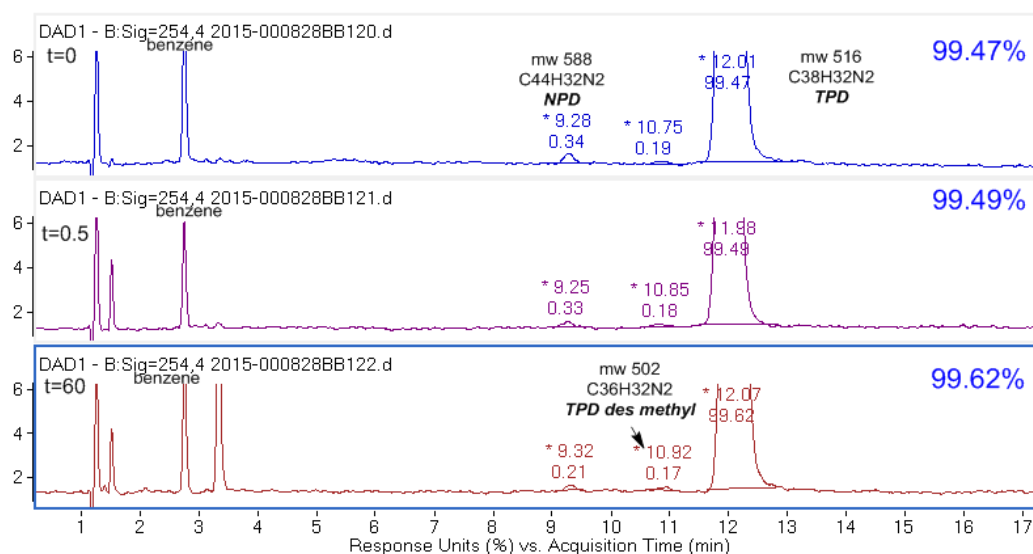


Figure S21. LC/MS chromatogram (top) of NPD, after 30 seconds exposure of a dilute (~1 mg/mL) benzene solution to a 450 watt medium pressure mercury vapor ultraviolet (UV) lamp (middle), and after 60 minutes exposure (bottom).

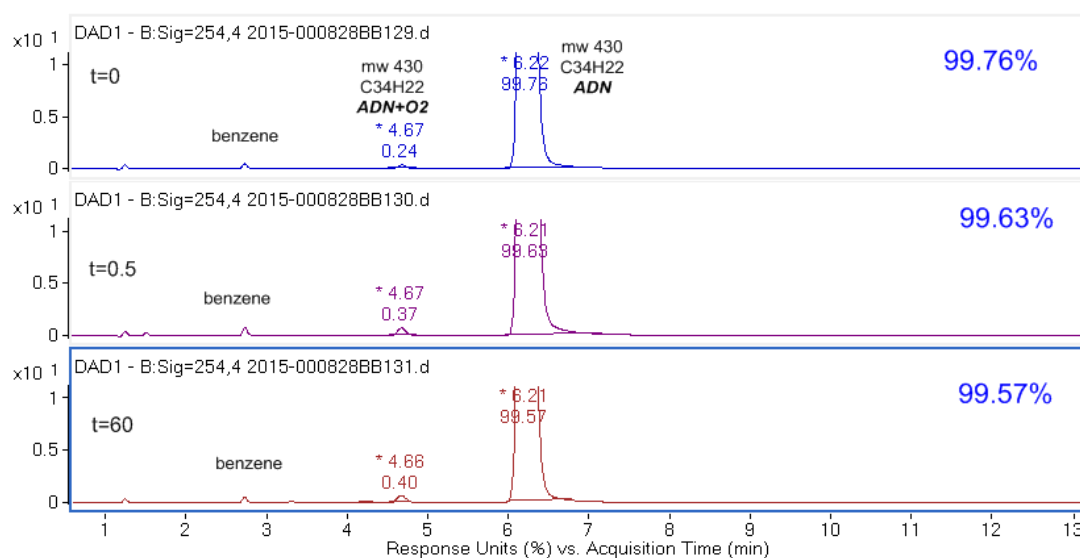


Figure S22. LC/MS chromatogram (top) of host material ADN, after 30 seconds exposure of a dilute (~1 mg/mL) benzene solution to a 450 watt medium pressure mercury vapor ultraviolet (UV) lamp (middle), and after 60 minutes exposure (bottom).

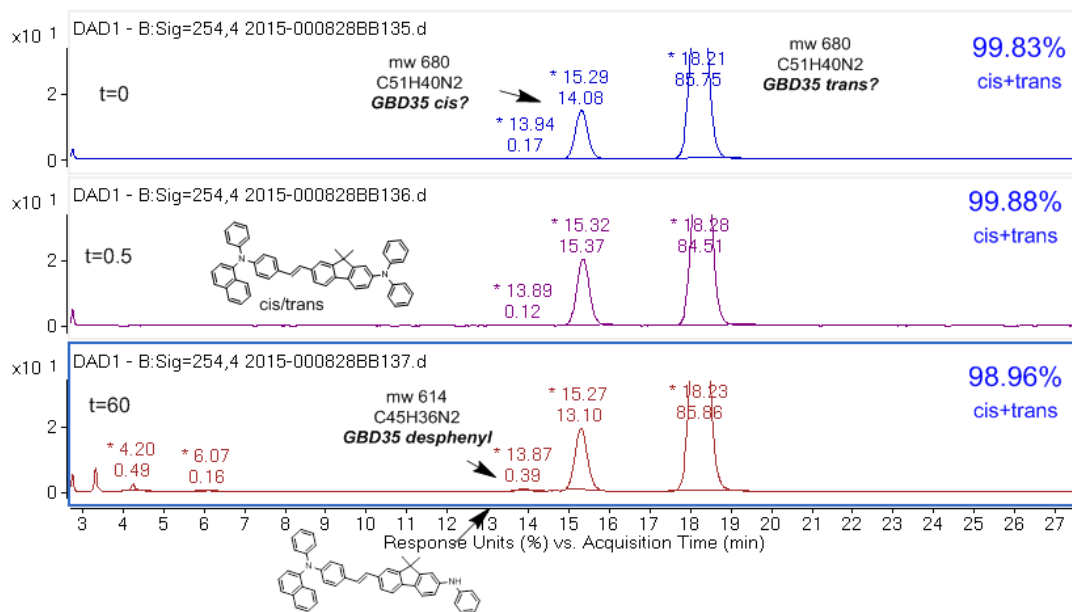


Figure S23. LC/MS chromatogram (top) of dopant **11**, after 30 seconds exposure of a dilute (~1 mg/mL) benzene solution to a 450 watt medium pressure mercury vapor ultraviolet (UV) lamp (middle), and after 60 minutes exposure (bottom).

CYCLIC VOLTAMMETRY OF **1**

Solution-phase cyclic voltammetry measurements were conducted using a WaveNano potentiostat (Pine Research Instrumentation). A silver/silver nitrate (silver wire immersed in a freshly prepared solution of 5 mM silver nitrate in anhydrous acetonitrile with 0.1 M TBAP as the supporting electrolyte), a platinum wire, and a platinum disk (1.6 mm diameter) were used as the reference, counter, and working electrodes, respectively. All oxidation scans were measured for approximately 5 mM solutions of analyte in DCM (anhydrous) with 1 M TBAP as the supporting electrolyte; all reduction scans for 5 mM solutions in THF (anhydrous, inhibitor-free) with 0.1 M TBAP. Typically at least 3 cycles (6 segments) were performed at a sweep rate of 20 mV/s. Energy levels were corrected by an offset of 4.7 V to convert to vacuum level. Shown below are 100-cycle repetitions of the oxidations (Figure S24) and reduction (Figure S25) of compound **1**.

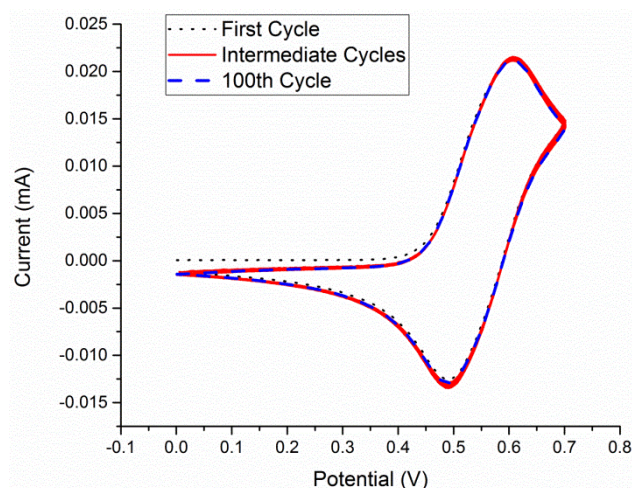


Figure S24. Repeated oxidations of **1** by cyclic voltammetry, with the first scan shown as a black dotted line, the 100th scan as a blue dashed line, and solid red lines for all intermediate scans.

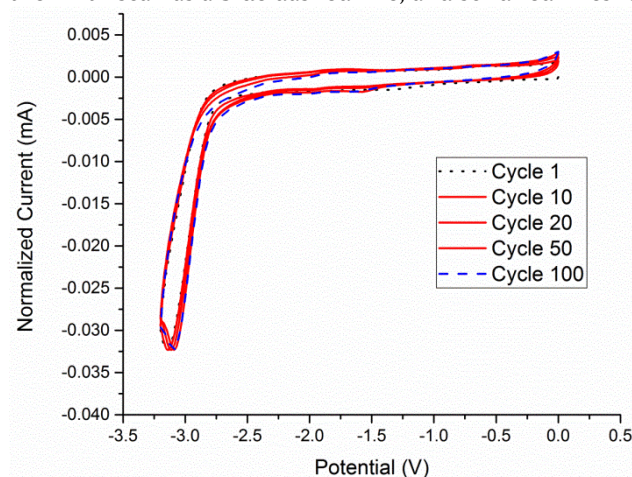


Figure S25. Repeated reductions of **1** by cyclic voltammetry, with the first scan shown as a black dotted line, the 100th scan as a blue dashed line, and solid red lines for selected scans inbetween.

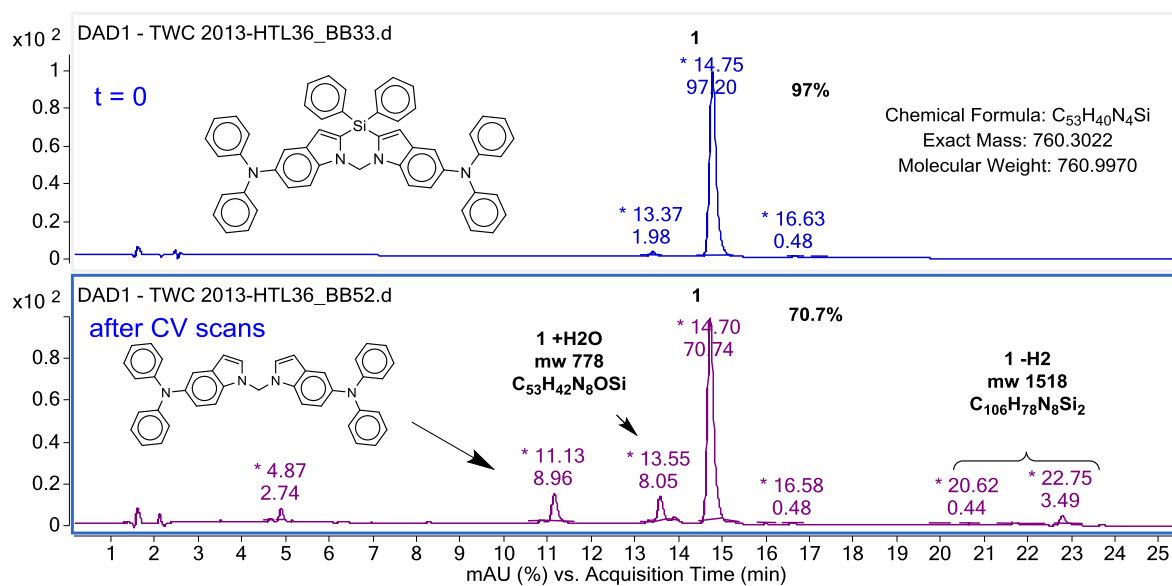


Figure S26. LC chromatograms of a solution of compound **1** in THF before (top) and after (bottom) subjection to extended electrochemical reduction, including identification of several peaks by MS.

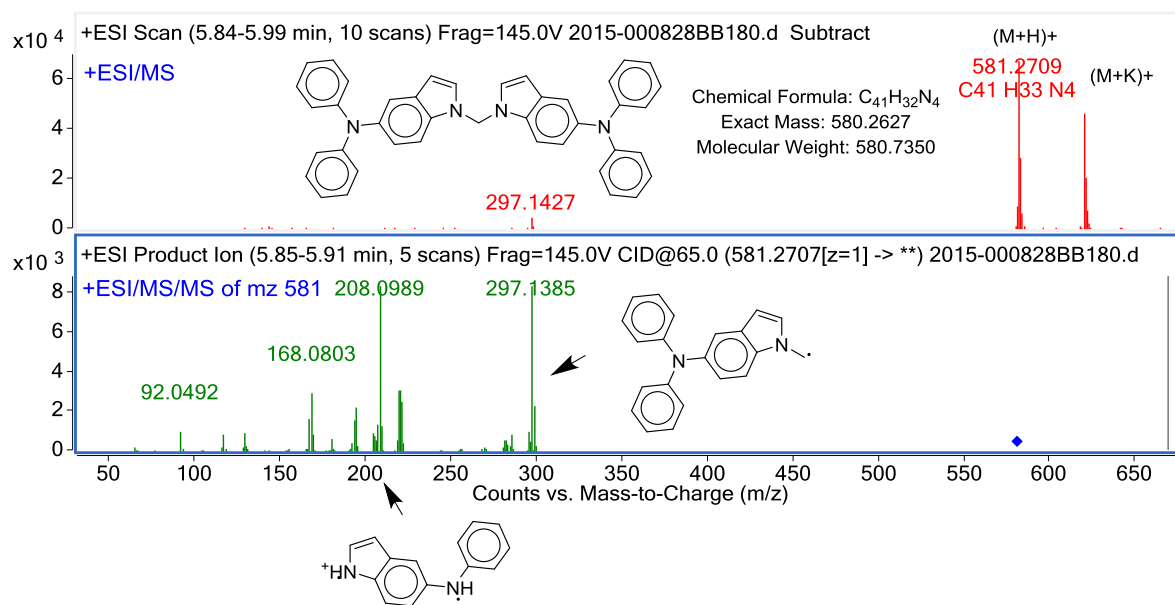


Figure S27. HRMS and tandem MS/MS of the peak at $m/z = 581$. Putative structure calculated as $M+H^+$ to have $m/z = 581.2705$, less than 1 ppm from the observed $m/z = 581.2709$.

PHOTOLUMINESCENCE SPECTROSCOPY OF COMPOUND **1**

Photoluminescence spectra of compound **1** diluted in 2-methyltetrahydrofuran (2-MeTHF) are shown in Figure S11. At room temperature, this compound fluoresces in the near-visible with λ_{max} centered near 405 nm. The onset indicates an S_1 energy of 3.28 eV. Upon cooling to 77 K, the emission profile changes: notably, the fluorescence narrows and gains some structure with an apparent shift in the maximum to 390 nm with a shoulder evident at slightly longer wavelengths (> 400 nm). This is commonly encountered on changing the matrix from a solution to a rigid glass, and it is worth noting that the S_1 energy is not significantly different at 77 K based on the fluorescence onset. The most notable feature is the appearance of a new structured emission profile with maxima at 457 and 482 nm and a slight shoulder at 520 nm. Time-gated experiments (Figure S28, blue dashed line) support assignment of this spectral feature to phosphorescence, emission from the triplet state. The onset indicates a T_1 energy of 2.81 eV.

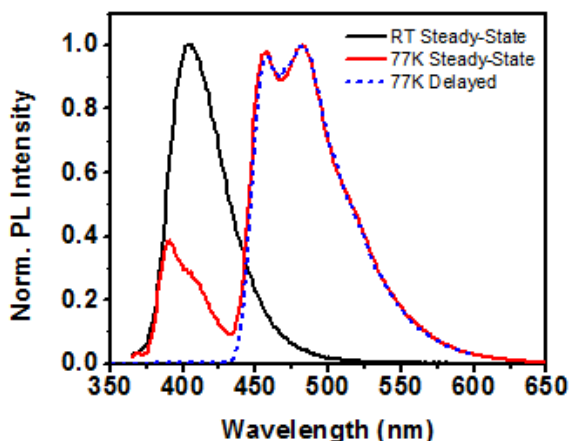


Figure S28. Photoluminescence spectra of **1** in 2-MeTHF (350 nm excitation).

Lowering the temperature to 77 K allows observation of phosphorescence, demonstrating that this molecule is capable of facile intersystem crossing upon singlet formation through optical excitation. At room temperature, the more temperature-dependent non-radiative processes likely outcompete the phosphorescent radiative decay. The lifetime of this triplet decay was estimated by observing the photoluminescent intensity of a sample real-time until the signal appeared to reach steady-state then manually closing the shutter from the source lamp and recording the decay (Figure S29). The data after closing the shutter were then fit to a simple exponential decay with good agreement providing a rate constant of 1.12 s^{-1} , or a lifetime of 890 ms at 77 K.

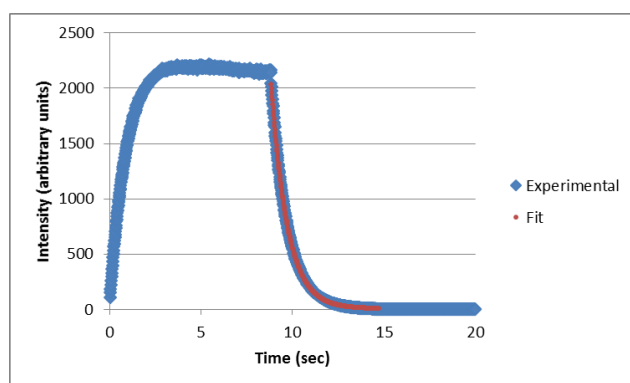


Figure S29. Decay of signal at 458 nm with excitation at 325 nm, sample of **1** in 2-MeTHF at 77K.

REFERENCES

- (1) Becke, A. D. A New Mixing of Hartree-Fock and Local Density-Functional Theories. *J. Chem. Phys.* **1993**, *98*, 1372.
- (2) Frisch, M. J.; Trucks, G. W.; Schlegel, H. B.; Scuseria, G. E.; Robb, M. A.; Cheeseman, J. R.; Montgomery, J. A., Jr.; Vreven, T.; Kudin, K. N.; Burant, J. C.; Millam, J. M.; Iyengar, S. S.; Tomasi, J.; Barone, V.; Mennucci, B.; Cossi, M.;

Scalmani, G.; Rega, N.; Petersson, G. A.; Nakatsuji, H.; Hada, M.; Ehara, M.; Toyota, K.; Fukuda, R.; Hasegawa, J.; Ishida, M.; Nakajima, T.; Honda, Y.; Kitao, O.; Nakai, H.; Klene, M.; Li, X.; Knox, J. E.; Hratchian, H. P.; Cross, J. B.; Bakken, V.; Adamo, C.; Jaramillo, J.; Gomperts, R.; Stratmann, R. E.; Yazyev, O.; Austin, A. J.; Cammi, R.; Pomelli, C.; Ochterski, J. W.; Ayala, P. Y.; Morokuma, K.; Voth, G. A.; Salvador, P.; Dannenberg, J. J.; Zakrzewski, V. G.; Dapprich, S.; Daniels, A. D.; Strain, M. C.; Farkas, O.; Malick, D. K.; Rabuck, A. D.; Raghavachari, K.; Foresman, J. B.; Ortiz, J. V.; Cui, Q.; Baboul, A. G.; Clifford, S.; Cioslowski, J.; Stefanov, B. B.; Liu, G.; Liashenko, A.; Piskorz, P.; Komaromi, I.; Martin, R. L.; Fox, D. J.; Keith, T.; Al-Laham, M.-A.; Peng, C. Y.; Nanayakkara, A.; Challacombe, M.; Gill, P. M. W.; Johnson, B.; Chen, W.; Wong, M. W.; Gonzalez, C.; Pople, J. A. *A.02 ed.*; Gaussian Inc.: Wallingford CT, 2009.